Kinetic study for the direct synthesis of dimethyl carbonate from methanol and CO_2 over CeO_2 at high pressure conditions

B.A.V. Santos, C.S.M. Pereira, V.M.T.M. Silva, J.M. Loureiro, A.E. Rodrigues *

Laboratory of Separation and Reaction Engineering, Department of Chemical Engineering, Faculty of Engineering of University of Porto, 4200-465 Porto, Portugal

ABSTRACT

The kinetics for the direct synthesis of dimethyl carbonate was studied over CeO_2 at high pressure conditions in a batch reactor. Langmuir–Hinshelwood and Eley–Rideal mechanisms were proposed and compared by the performance of the respective reaction rate expression in fitting to the experimental kinetic data. The reactions were held at different temperatures (378–408 K), CO_2/methanol molar ratios (1.1–4.0) and pressures (15–20 MPa) in order to adjust the kinetic parameters. An activation energy of 106 kJ mol^{-1}, as well as the standard enthalpy and Gibbs energy of reaction (−20.10 and 31.50 kJ mol^{-1}) were calculated from experiments. Furthermore, the changes in pressure revealed an effect on the kinetic constant, with an activation volume equal to −0.208 cm^3 mol^{-1}.

© 2013 Elsevier B.V. All rights reserved.

1. Introduction

Dimethyl carbonate (DMC) is a promising chemical for green chemistry processes due to its high versatility and low toxicity [1]. DMC is considered a build block for organic chemical synthesis, having specially importance for replacing the hazardous and toxic phosgene and dimethyl sulphate or methyl halide in carbonylation and methylation reactions [2,3]. It can also be used as reactant for the synthesis of diphenyl carbonate [4] or glycol carbonate [5], which are useful for polymers production. DMC has also benign properties to become an alternative to conventional solvents [6], reducing the VOCs and particles emissions; or even be used as gasoline additive [7], due to its blending properties and high oxygen content (53.3%), reducing the particles and NOx emissions.

However, in order to be considered a green chemical, DMC ought to be produced by a green process as well. Until 1980, DMC was produced by phosgenation of methanol (MeOH) [1], which was abandoned due to the high toxicity of phosgene. Nowadays, it is produced mainly by oxy-carbonylation of MeOH [8] and carbonylation of methylnitrile [9], although those routes use toxic and corrosive chemicals. Therefore, new alternatives have been developed such as the transesterification of ethylene

carbonate [10–12], transesterification of methylcarbamate [13], or the direct synthesis from CO_2 and MeOH [14–16]. In the work of Leino et al. [14] a comparative review for conventional versus direct synthesis method for dialkylcarbonates is presented. The direct synthesis ($CO_2 + 2MeOH \leftrightarrow DMC + H_2O$) is considered to be one of the most promising routes for DMC production based on economical and environmental features [17]. However, this route shows high thermodynamic limitations even at high pressure conditions as concluded from our previous work [18]. Several approaches have been studied in order to overcome this issue, such as the use of dehydrating agents, which will react with the water, to shift the equilibrium towards the DMC production: ketals (0.5–200 MPa, 383–453 K, 24 h, conv./selec.: 1.5–88/60–100%) [19–24], orthoesters (30 MPa, 453 K, 24 h, conv./selec.: 20/93%) [25], acetonitrile (0.5 MPa, 423 K, 2 h, conv./selec.: 3.5/95%) [26,27], benzonitrile (0.5 MPa, 423 K, 2 h, conv./selec.: 9.4/99%) [28], butylene oxide (9 MPa, 423 K, 8 h, conv./selec.: 12/80%) [29], or ionic liquids (9 MPa, 393 K, 9 h, conv./selec.: 12/90%) [30]. The decrease of selectivity and the need of removing the side products are pointed as the major drawbacks for this approach. In alternative, Choi et al. [31] reached a DMC yield around 40% by removing the water with molecular sieve 3 A in an external cooled loop, reaching similar yields as with dehydrating agents.

Apart from the thermodynamic limitations, carbon dioxide is also a stable molecule with low reactivity leading to low reaction rates. The direct synthesis of DMC is achieved in the presence of an acid–base catalyst. While strong basicity is recommended to improve the activation of CO_2, strong acidity could lead to the dehydration of methanol [32]. On the basic site CO_2 is activated and methoxy groups are formed from MeOH, while the methyl

Symbols

$\Delta_r C_p^{\circ}$	heat capacity change of reaction $[\text{J mol}^{-1}\,\text{K}^{-1}]$
E_a	activation energy $[\text{J mol}^{-1}]$
f_i°	standard fugacity of pure species i [Pa]
$\hat{f}_I$	fugacity of species i in the mixture [Pa]
F_{obj}	objective function
$\Delta_r G_{T_0}^{\circ}$	Gibbs energy change of reaction $[\text{J mol}^{-1}]$
$\Delta_r H_{T_0}^{\circ}$	enthalpy change of reaction $[\text{J mol}^{-1}]$
k	kinetic constant $[\text{g}^{-1}\,\text{min}^{-1}]$
k_0	pre-exponential factor of kinetic constant $[\text{g}^{-1}\,\text{min}^{-1}]$
$K_{ads,i}$	adsorption constant
K_{eq}	equilibrium constant
m_{cat}	catalyst mass [g]
P, P°, P_i	pressure, standard pressure, partial pressure [Pa]
$\hat{\varphi}_i$	fugacity coefficient of species i
r	reaction rate $[\text{min}^{-1}]$
R	ideal gas constant $[\text{J mol}^{-1}\,\text{K}^{-1}]$
t	time [min]
T	temperature [K]
$\Delta v^{\#}$	activation volume $[\text{m}^3\,\text{mol}^{-1}]$
x	molar fraction
X_c	molar reaction conversion

groups are produced on the acidic site [33,34]. Organometallic complexes, in particular dibutyltin dimethoxy ($Bu_2Sn(OMe)_2$), show high selectivity for DMC synthesis [35,36]; however, these catalysts have low activity mainly due to the deactivation in presence of water. Furthermore, heterogeneous catalysts are more environmentally-friendly because they can be easily separated from the reaction mixture avoiding the use of hazardous solvents and more energetic-cost processes.

Tomishige et al. [37] reported the direct synthesis of DMC over ZrO_2 with high selectivity. Afterwards, more efforts have been done in order to find an efficient heterogeneous catalyst for this route: Table 1 shows novel catalysts for this route. In spite of the large variety of catalysts, those based on ZrO_2 and/or CeO_2 are still showing the higher selectivity, which is due to the acid–base properties of these catalysts [38]. The best results were achieved using CeO_2 combined with other oxides such as ZrO_2 [23] or TiO_2 [39]; furthermore, the modification of ceria based catalyst with H_3PO_4 [40,41], $H_3PW_{12}O_{40}$ [39,42], Ga_2O_3 [43] or Al_2O_3 [44] have also contributed for the improvement of acid–base properties of the catalyst and improvement of ceria stabilization avoiding the reduction of Ce^{4+} to Ce^{3+}, which is the main cause of ceria based catalyst deactivation [44].

In spite of the huge efforts done in searching for novel catalysts and dehydrating agents, few studies present kinetic data [55,56], which is essential to design and evaluate novel processes for DMC production and turn this route competitive in comparison with the conventional processes. In this work, it will be presented a detailed kinetic and equilibrium model for the direct synthesis over CeO_2 at high pressure conditions. CeO_2 was chosen as catalyst since besides the good results already achieved for this reaction it is commercially available or it can be easily prepared by calcination of cerium hydroxide with good reproducibility. Two reaction rate expressions will be considered based on Langmuir–Hinshelwood and Eley–Rideal mechanisms. It will be studied the effect of several parameters on the reaction rate: temperature, initial CO_2/MeOH ratio and pressure in order to adjust the kinetic parameters.

2. Experimental

2.1. Materials

Cerium oxide was prepared from cerium hydroxide ($Ce(OH)_4$, Sigma–Aldrich®) by calcination. Anhydrous methanol (99.9%, AcroSeal®), CO_2 (99.995%, Linde®) and dimethyl carbonate (99%, Sigma–Aldrich®) were used without further purification. The water used was deionised.

2.2. Analytical method

All the samples were analyzed by GC chromatography (GC2010 plus, Shimadzu®) using a fused silica capillary column, Chrompack CP-Wax 52 CB (25 m × 0.25 mm × 1.2 μm) to separate the compounds coupled with TCD and FID detectors. Helium N50 was used as carrier gas at a constant linear velocity of 30 cm s^{-1} with a split ratio equal to 30 for 2 μL of sample injected. The temperature of the injector and the detectors were set at 573 K, while the oven temperature was set at 348 K during 5 min of analyzing time.

Table 1
Heterogeneous catalysts for the direct synthesis of DMC.

Catalyst	Operating conditions	Time	Yield/selec.	Ref.	Year
ZrO_2	433 K	2 h	0.3/100%	[37]	2000
$Ni(CH_3COO)_2 \cdot 4H_2O$	413 K; 7.0 MPa	12 h	2.1/45%	[45]	2000
H_3PO_4/ZrO_2	403 K	2 h	0.3/100%	[41]	2000
H_3PO_4/ZrO_2	403 K	2 h	0.3/100%	[40]	2001
CeO_2–ZrO_2	383 K; 6.0 MPa	4 h	0.8/100%	[23]	2002
H_3PO_4/V_2O_5	453 K; 0.6 MPa	–[a]	1.8/93%	[46]	2005
Cu–Ni/V_2O_5–SiO_2	413 K; 0.9 MPa	–[a]	2.4/87%	[47]	2006
CeO_2	403 K	5 h	0.8/100%	[48]	2006
Cu (Ni, V, O) [b]	393 K; 1.2 MPa	–	4.5/90%	[49]	2007
Cu (Ni, V, O)	393 K; 1.2 MPa	–	3.5/93%	[49]	2007
$H_3PW_{12}O_{40}/Ce_{0.1}Ti_{0.9}O_2$	443 K	12 h	5/100%	[39]	2007
Al_2O_3/CeO_2	408 K; 5.0 MPa	3 h	0.4/100%	[44]	2007
ZrO_2/SiO_2	423 K; 20 MPa	80 h	6[c]/100%	[50]	2010
$CuCl_2/AC$	398 K; 1.2 MPa	4 h[b]	–/90%	[51]	2010
$Co_{1.5}PW_{12}O_{40}$	353 K; 0.25 MPa	5 h	1.1/69%	[52]	2010
$Co_{1.5}PW_{12}O_{40}$	473 K; 0.1 MPa	–[b]	7.6/86.5%	[53]	2010
$H_3PW_{12}O_{40}/Ce_{0.6}Zr_{0.4}O_2$	443 K; 6.0 MPa	3 h	1.2/100%	[42]	2011
$5Ga_2O_3/Ce_{0.6}Zr_{0.4}O_2$	443 K; 6.0 MPa	3 h	2.3/100%	[43]	2011
Cu–Ni/GNS	373 K; 1.2 bar	3 h[b]	5/92%	[54]	2011

[a] Continuous reactor.
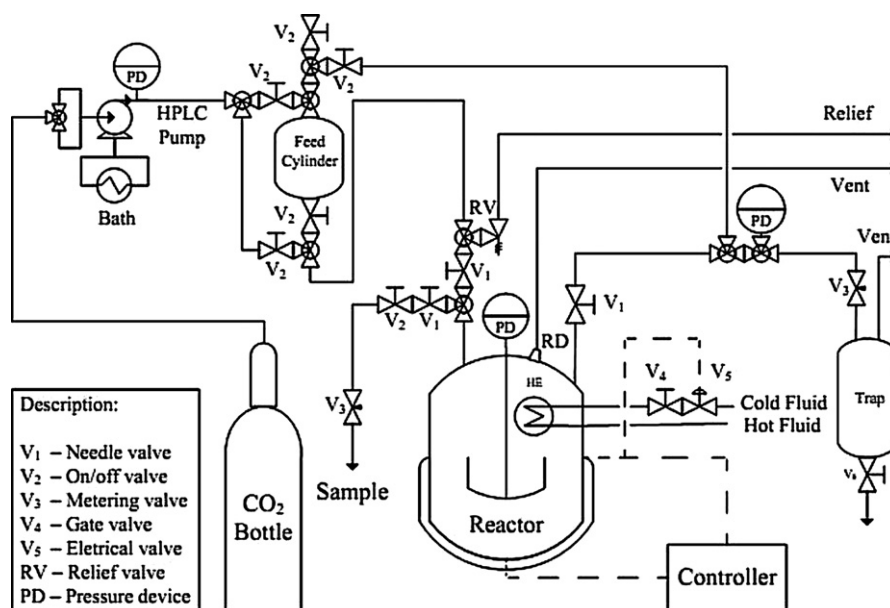[b] UV radiation.
[c] DMC/cat. molar ratio.

Fig. 1. Sketch of the experimental set-up for high pressure reactions.

2.3. Experimental set-up

Fig. 1 shows the sketch of the experimental set-up where all the experiments were conducted. The set-up is composed by an auto-clave reactor (HP reactor 4575A, Parr®) coupled with temperature (±1 K) and stirrer speed control, and a pressure gauge (±0.01 MPa) (4848 reactor controller, Parr®); the HPLC pump (K-1900 100 mL head, Knauer®) is cooled with an external cooling bath at 278 K in order to keep CO_2 in the liquid state; the feed cylinder is used to add other chemicals to the reactor through the CO_2 stream. The depressurization of the system is easily done through a metering valve into a trap cylinder to expand the CO_2; moreover, the valve is heated by an external resistance thereby avoiding freezing.

2.4. Experimental procedure

The catalyst is firstly added to the reactor and then the reactor is closed; the loss of catalyst is avoided by the use of a filter. Then the reactor is filled with CO_2, through the feed cylinder, at environmental temperature around 1 MPa and heated until 413 K, followed by depressurization. This procedure is used to reduce the initial water content in the reactor, which is present on the tubes and reactor walls. With this approach it was reached an average of initial water contents around 0.5% for all the experiments performed. Afterwards, the methanol is dragged through the feed cylinder by the CO_2 stream. Finally, the temperature is set followed by the pressurization with CO_2 to the desired pressure. The samples are carefully collected through the sample line (2 mL) by a metering valve to reach a slow depressurization and a complete condensed sample (without CO_2). Then the pressure drop (around 0.4 MPa for each sample) is compensated with CO_2 that also cleans the dead volume for the next sample. In the end of the reaction, the reaction mixture is cooled until 300 K and the reactor is slowly depressurized improving the condensation of the reaction mixture (without CO_2).

Six standard solutions (50–60 mL), with known concentrations of DMC, from 0.10 to 0.30%, diluted on MeOH were added to the reactor with the purpose of validating the sampling. Two samples were collected: one from the sampling line and other after depressurization. Both methods showed good agreement with the real concentration inside the reactor, with an average absolute deviation of 0.03%. A typical experiment is carried out at 403 K, pressurized with CO_2 at 20 MPa with 50 mL of MeOH and 4.5 g of catalyst. Table 2 presents the reaction operating conditions held

Table 2
Experimental conditions for kinetic and/or equilibrium experiments.

Run	T/K	P/MPa	$nCO_2/nMeOH$	$x_{H_2O}^{initial}$ % (CO_2 free basis)	$m_{Catalyst}$/g	Stirrer/rpm
1	398	20.0	2.5	0.42	4.6	200
2	398	20.0	2.5	0.57	4.6	200
3	398	20.0	2.5	0.34	4.6	400
4	408	20.0	2.4	0.72	4.4	200
5	403	20.0	2.5	0.35	4.6	200
6	393	20.0	2.6	0.56	4.6	200
7	388	20.0	2.7	0.57	4.7	200
8	388	20.0	2.7	0.37	4.7	200
9	383	20.0	2.9	0.58	4.6	200
10	378	20.0	2.9	0.74	4.4	200
11	398	20.0	1.1	0.17	4.7	200
12	398	20.0	1.6	0.18	4.6	200
13	398	20.0	1.8	0.28	4.6	200
14	398	20.0	4.0	1.06	4.6	200
15	398	20.0	4.0	0.78	4.5	200
16	398	17.5	2.5	0.54	4.6	200
17	398	15.0	2.5	0.86	4.5	200
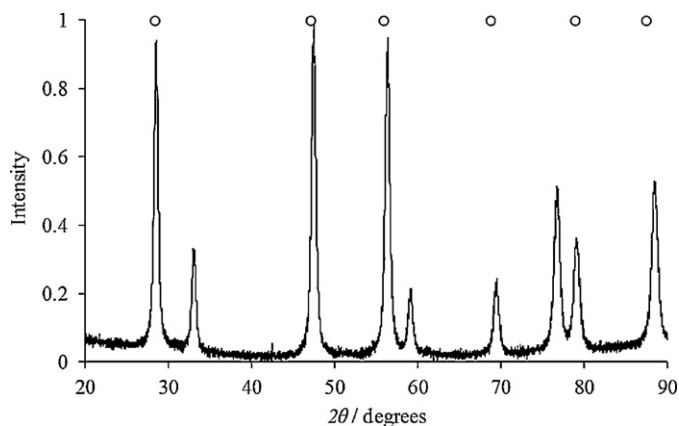
Fig. 2. XRD patterns of CeO$_2$ prepared by calcination. Crystal structure: fluorite ($\bigcirc$).

Fig. 3. Reproducibility: experimental DMC molar fraction along the time. Reaction conditions: 20 MPa, 398 K, 200 rpm, 4.6 g CeO$_2$, nCO$_2$/nMeOH: 2.54/1.

for all the experiments. Several experiments were carried out with the objective of studying the effect of different physical parameters on the reaction rate and/or equilibrium yield: external mass transfer (200 and 400 rpm), temperature (378–408 K), CO$_2$/MeOH molar ratio (1.1–4.0) and pressure (15–20 MPa).

3. Results

3.1. Catalyst characterization

As mentioned before, our catalyst, CeO$_2$, was prepared by calcination of cerium hydroxide, Ce(OH)$_4$, as reported by Yoshida et al. [48]. They observed that above 873 K the reaction rate was proportional to the surface area; however for 673 K the activity was lower than expected, probably due to insufficient water removal. The calcination temperature should be as low as possible in order to minimize the decrease of surface area by sinterization but ensuring the maximum water removal. The thermogravimetric analysis, for Ce(OH)$_4$, showed a complete water loss above 900 K. Therefore, after increasing the temperature at a rate of 5 K min^{-1}, CeO$_2$ was calcined at 923 K during 4 h, in order to guarantee a complete water removal. Furthermore, a BET area of 36 m^2 g^{-1} was determined, which is in accordance with the values reported at this temperature using Ce(OH)$_4$ as a precursor [48].

Fig. 2 shows the X-ray diffraction patterns for CeO$_2$ calcined at 923 K. The diagram reveals crystallinity similar to fluorite structure, as expected, with low crystallinity. The low crystallinity was also observed by Yoshida et al. [48]. They observed an increase of crystallinity with the increase of temperature, although the increase of temperature leads to a decrease of surface area.

3.2. Reproducibility and external resistance to mass transfer

In order to evaluate the reproducibility of our experiments, two reactions were carried out at almost the same operating conditions (Table 2). The small difference in the initial water contents between the two reactions has negligible effect on the initial reaction rate. The DMC molar fractions along the time for these two experiments are depicted in Fig. 3. It can be observed a good reproducibility since the curves are coincident within experimental errors.

Then, in order to evaluate the external mass transfer resistance, two reactions were held at the same conditions, again with small differences in the initial water content, but varying the stirrer speed. Fig. 4 shows the DMC produced along time. Since, in both runs, the initial reaction rates are similar, the external resistance to mass transfer is negligible above 200 rpm.
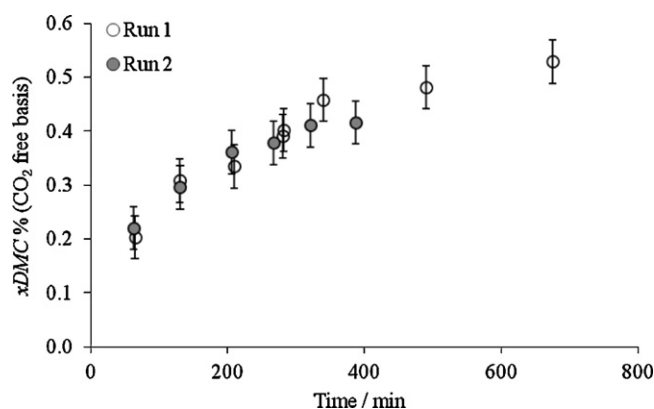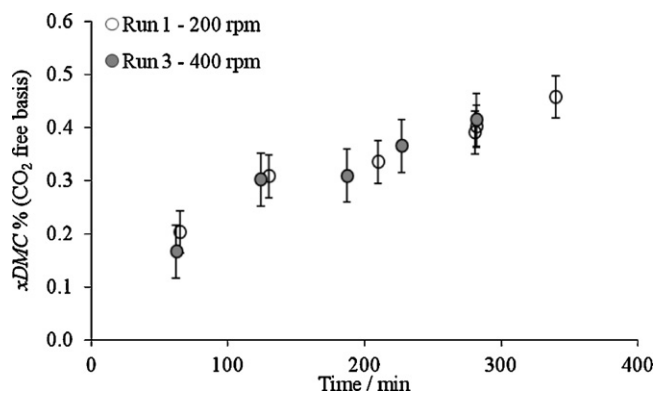

Fig. 4. Experimental DMC molar fraction along the time for different stirrer speed. Reaction conditions: 20 MPa, 398 K, 4.6 g CeO$_2$, nCO$_2$/nMeOH: 2.54/1.

3.3. Chemical equilibrium

Once guaranteed good reproducibility and negligible external mass transfer resistance, the kinetic modelling can be optimized; however, the reaction equilibrium data is needed for the kinetic model. In our previous work [18] we reported some reaction equilibrium data at high pressure conditions. Herein is presented a deeper study for the reaction equilibrium, varying the temperature, CO$_2$/MeOH molar ratio and pressure. The equilibrium constant can be calculated based on the fugacity of each compound ($\widehat{f}_i$) by the following equation [57]:

$$K_{eq} = \prod_{i=1}^{NC} \left(\frac{\widehat{f}_i}{f_i^\circ} \right)^{\theta_i} = \prod_{i=1}^{NC} \left(\frac{x_i \cdot \widehat{\varphi}_i \cdot P}{P^\circ} \right)^{\theta_i} \tag{1}$$

For ideal gas the fugacity coefficient is equal to one ($\widehat{\varphi}_i = 1$). Besides, the equilibrium constant can also be calculated based on the thermodynamic properties of reaction (standard enthalpy ($\Delta_r H_{T_0}^\circ$)), Gibbs energy ($\Delta_r H_{T_0}^\circ$) and heat capacity ($\Delta_r C_p^\circ$) change of reaction):

$$\ln K_{eq} = \left[\frac{-\Delta_r G_{T_0}^\circ}{R \cdot T_0} \right] + \left[\frac{\Delta_r H_{T_0}^\circ}{R \cdot T_0} \left(1 - \frac{T_0}{T} \right) \right]$$
$$+ \left[-\frac{1}{R \cdot T} \int_{T_0}^{T} \Delta_r C_p^\circ \cdot dT + \frac{1}{R} \int_{T_0}^{T} \frac{\Delta_r C_p^\circ}{T} \cdot dT \right] \tag{2}$$

In the present work the enthalpy and Gibbs energy of reaction are adjusted from our experimental data for ideal and real gas mixture by minimization of the maximum relative deviation (Eq. (3)).

Table 3
Standard enthalpy and Gibbs energy change of reaction: adjusted from our reaction equilibrium data.

Model	$\Delta_r H^\circ_{T_0}$/kJ mol^{-1}	$\Delta_r G^\circ_{T_0}$/kJ mol^{-1}
Ideal gas	-20 ± 2	31 ± 1
Real gas (SRK/mHV2)	-22 ± 3	32 ± 1

This objective function gives a more homogenous distribution of the relative deviation.

$$F_{\text{obj}} = \min \left\{ \max \left[\frac{|x_{\text{DMC}}^{\text{model}} - x_{\text{DMC}}^{\text{exp.}}|}{x_{\text{DMC}}^{\text{exp.}}} \right] \right\} \tag{3}$$

The Soave–Redlich–Kwong (SRK) equation of state coupled with the modified Huron–Vidal second order (mHV2) mixing rule was used to describe the fugacity of the real gas, with the binary energetic parameter optimized in our previous work [18]. All the other physical properties were collected from DIPPRTM. Table 3 contains the enthalpy and Gibbs energy of reaction adjusted for ideal and real gas; note that these values are slightly different from the predicted by Hofmann et al. [56], −17.99 and 37.31 kJ mol^{-1}, respectively.

The experimental DMC molar fractions at equilibrium conditions as well as the values estimated by both the ideal and real gas models are shown in Table 4. Contrarily to the expected, considering an ideal gas mixture leads to a lower deviation than using SRK/mHV2 to predict the fugacity. This may be explained due to the deviation of the real gas model at supercritical conditions, since the model was adjusted based on liquid–vapour equilibrium, at temperatures and pressures below the critical point of the mixture.

3.4. Mechanisms and kinetic models

Two mechanisms were considered for the direct synthesis of DMC over acid–base catalysts: Eley–Rideal and Langmuir–Hinshelwood mechanism. The Eley–Rideal mechanism was successfully used to model the kinetics of the direct synthesis of DMC using butylene oxide as dehydrating agent over ZrO_2–MgO [55]. This mechanism was based on in situ infrared spectroscopy [33,58]; in this work the formation of an intermediate species, methyl carbonate (MC), over zirconia, was observed. However, this mechanism does not consider the adsorption of CO_2 over the catalyst as an important step; it is assumed that the CO_2 reacts directly with the methoxy group adsorbed on the catalyst (Zr–OCH_3) since the adsorption of MeOH seems to be much stronger. Tomishige et al. [34] proposed the formation of methyl carbonate from CO_2 and the methoxy group, both adsorbed on the catalyst. In order to have a comparison with this mechanism, the Langmuir–Hinshelwood mechanism was proposed since it considers the adsorption of all species on the catalyst and also because this mechanism has been successfully fitted to several reactions. The two reaction mechanisms proposed are shown in Table 5; moreover, the reaction rate expression can be obtained from the reaction mechanism [59].

Table 5
Reaction mechanism based on Langmuir–Hinshelwood and Eley–Rideal methodology.

Step	Mechanism 1	Mechanism 2 [55]
1	$CO_2 + ^* \leftrightarrow CO_2^*$	$MeOH + ^* \leftrightarrow MeOH^*$
2	$MeOH + ^* \leftrightarrow MeOH^*$	$MeOH^* + CO_2 \leftrightarrow MC^*$
3	$2MeOH^* + CO_2^* \leftrightarrow DMC^* + H_2O^* + ^*$	$MC^* + MeOH^* \leftrightarrow DMC + H_2O + ^*$
4	$DMC^* \leftrightarrow DMC + ^*$	
5	$H_2O^* \leftrightarrow H_2O + ^*$	
	Controlling step: 3	Controlling step: 2

* Active centre.

The reaction rate expressions (r/min^{-1}) can be deduced from the mechanisms considering each step as an elementary reaction and defining the controlling step. Eqs. (4) and (5) express the reaction rates, for mechanisms 1 and 2, respectively, as function of the kinetic constant (k), catalyst mass (m_{cat}), partial pressure (P_i), standard pressure (P°), adsorption constants (K_{ads}) and (global) reaction equilibrium constant (K_{eq}).

$$r = \frac{m_{\text{cat}} \cdot k \cdot \left\lfloor P_{CO_2} \cdot P_{\text{MeOH}}^2 - \left(P_{\text{DMC}} \cdot P_{H_2O} / K_{\text{eq}} / P^\circ \right) \right\rfloor}{\left[1 + \sum K_{\text{ads},i} \cdot \left(P/P^\circ \right) \right]^3} \tag{4}$$

$$r = \frac{m_{\text{cat}} \cdot k \cdot \left\lfloor P_{CO_2} \cdot P_{\text{MeOH}}^2 - \left(P_{\text{DMC}} \cdot P_{H_2O} / K_{\text{eq}} / P^\circ \right) \right\rfloor}{\left(P_{\text{MeOH}} / P^\circ \right) \left[1 + K_{\text{ads},1} \cdot \left(P_{\text{MeOH}} / P^\circ \right) + K_{\text{ads},2} \cdot \left(P_{\text{MeOH}} / P^\circ \right) \cdot \left(P_{CO_2} / P^\circ \right) \right]} \tag{5}$$

The adsorption constants were considered as not depending of temperature for the studied temperatures range, because a large number of parameters drastically increases the complexity of the optimization and may lead to unrealistic values for the adsorption enthalpy. These values ought to be measured by adsorption experiments. However, the kinetic constant was considered function of temperature following an Arrhenius equation:

$$k = k_0 \cdot e^{-E_a/RT} \tag{6}$$

The activation energy (E_a) reflects the effect of temperature on the reaction rate; k_0 is the pre-exponential factor. For a batch reaction the dependence of molar reaction conversion (X_c) with time is expressed by the following equation:

$$\frac{dX_c}{dt} = r, \quad \text{Initial condition}: X_c(t = 0) = 0 \tag{7}$$

3.5. Parameters optimization

The kinetic parameters were adjusted from the experimental data by minimization of the maximum average deviation of each reaction experiment (Eq. (8)). Furthermore, bootstrapping technique was used in order to estimate the parameters errors [60].

Among the experiments shown in Table 2, just some were used for parameters optimization (Runs 1–3, 6, 8, 11–15); the others were used only for equilibrium purposes, or to measure the initial reaction rate (lowest temperature); the pressure effect was not
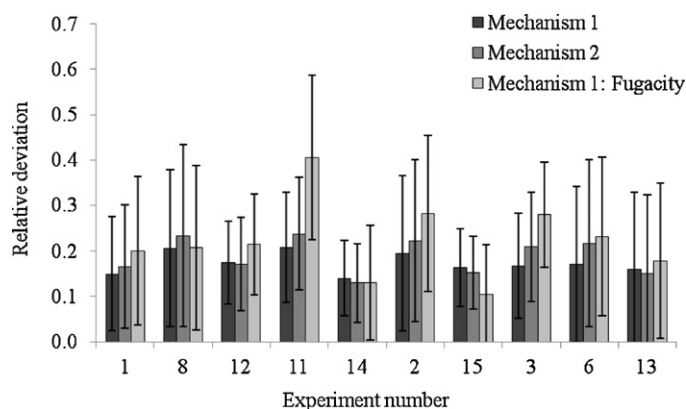
Table 4
Experimental and predicted DMC molar fractions (CO_2 free basis) at equilibrium for several reaction conditions.

Run	x_{DMC}% Experimental	Equilibrium conversion (%)	x_{DMC}% Ideal gas	Relative deviation (%)	x_{DMC}% Real gas	Relative deviation (%)
1	0.57	1.1	0.52	−9.5	0.50	−13.9
4	0.33	0.7	0.37	11.3	0.35	6.4
5	0.57	1.1	0.52	−10.5	0.49	−15.3
6	0.52	1.0	0.51	−3.0	0.49	−7.2
7	0.59	1.2	0.54	−10.1	0.51	−14.7
12	0.58	1.2	0.56	−2.9	0.64	9.2
13	0.51	1.0	0.54	5.4	0.59	12.9
15	0.39	0.8	0.44	12.2	0.35	−10.3
16	0.43	0.9	0.44	1.8	0.43	0.6
17	0.33	0.7	0.31	−5.6	0.31	−5.0

Fig. 5. Average deviation from the experimental data for each experiment.

Fig. 6. Arrhenius plot: logarithm of initial reaction rate as function of the inverse of temperature.

taken into account for these parameters optimization but only to evaluate its effect afterwards.

$$F_{obj} = \min \left\{ \max \left[\sum_{i=1}^{NP} \left(\frac{|x_{DMC}^{model} - x_{DMC}^{exp.}|/x_{DMC}^{exp.}}{NP} \right) \right] \right\} \quad (8)$$

The ordinary differential equation, which constitutes an initial value problem, was solved using a Runge–Kutta method implemented in Matlab® (subroutine ODE45). Fig. 5 shows the average deviation, as well the standard deviation, for mechanisms 1 and 2; furthermore, the model based on mechanism 1 was optimized considering a real gas ($\hat{f}_i \leftrightarrow P_i$) since mechanism 1 showed higher performance in fitting the model to the experimental data, the fugacity of the real gas was also estimated using the SRK/mHV2 model, optimized in our previous work. However, the ideal gas model showed better results than considering a real gas; once again this may be explained by the fact that reactions were conducted above the critical point.

The kinetic parameters optimized from the experimental data and the respective errors are shown in Table 6. Some parameters were neglected due to its high error (>100%) and also because their low effect on the performance of the model: $K_{ads,3}$ and $K_{ads,4}$ (H_2O and DMC adsorption constants) for mechanism 1 and the $K_{ads,2}$ for mechanism 2. For the three models the activation energy was between 101 and 117 kJ mol^{-1}, which is higher than the reported by Hoffmann et al. [56] for CeO_2–ZrO_2 (Ce 80%), which is around 75 kJ mol^{-1}. The large difference on the activation energy between the two catalysts was possibly caused by the difference of the acid–base properties, which are affected by the ZrO_2 content and synthesis conditions [38]. The acidity and basicity are directly related to the catalyst activity [42,43].

The activation energy obtained for the model based on mechanism 1 for ideal gas (106 kJ mol^{-1}) was similar to the estimated by the Arrhenius plot for the initial reaction rate (107 kJ mol^{-1}). Fig. 6 shows the respective Arrhenius plot, where the initial reaction rate was calculated by the slope of the linear line fitted to the first reaction experimental points.
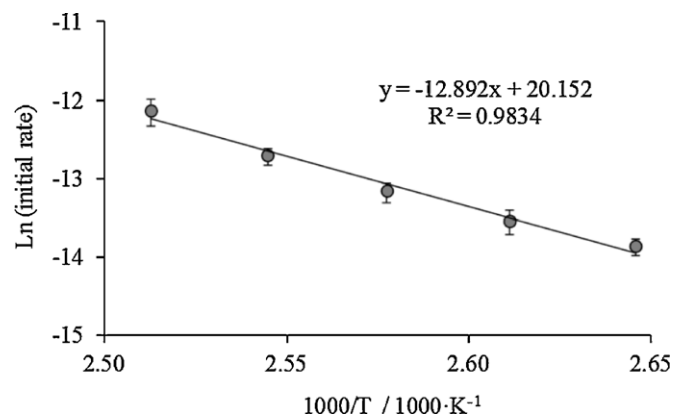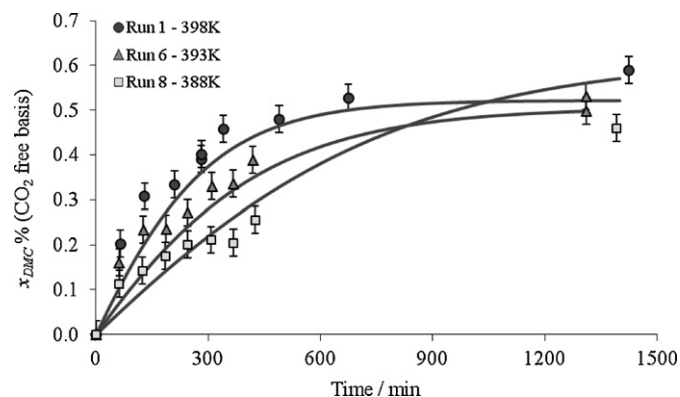

Fig. 7. Experimental DMC molar fraction along the time at different temperatures. Reaction conditions (approx.): 20.0 MPa, 200 rpm, 4.6 g CeO_2, $nCO_2/nMeOH$: 2.6/1.

3.6. Simulation results

Herein are presented the main simulation results for the kinetic modelling at high pressure conditions. The evolution of DMC molar fraction along the time at three different temperatures is depicted in Fig. 7. It can be observed from the graph a good fitting for the experimental data, with exception of the last point for 388 K. The major drawback in the experiments is the estimation of the initial amount of water that is predicted based on the final amounts of water and DMC, since there is some water present on the walls of the tubes and vessel that are mixed with the stream of MeOH and CO_2. Thus, this uncertainty may lead to relative high deviations for the equilibrium, which also explains some deviations observed on the equilibrium prediction. However, this has almost no effect on the initial reaction rate as predicted from the model. The DMC molar fractions as function of time for 4 different CO_2/MeOH molar ratios are shown in Fig. 8. These results are the most important to validate the reaction rate expression, while the variation of temperature is mainly useful for the determination of the activation energy almost independently of the reaction rate expression.

It can be concluded that the model shows a reasonable fitting to the experimental data considering that the experiments were

Table 6
Kinetic parameters optimized from the kinetic experiments.

Model	E_a/kJ mol^{-1}	Error (%)	k_0/min^{-1}	Error (%)	$K_{ads,1}$	Error (%)	$K_{ads,2}$	Error (%)	Mean deviation (%)
Mechanism 1	106	1	0.8	21	9	26	109	9	17
Mechanism 2	117	1	21	28	173	16	–	–	19
Mechanism 1: Fugacity	101	1	9	34	0.2	34	994	9	22

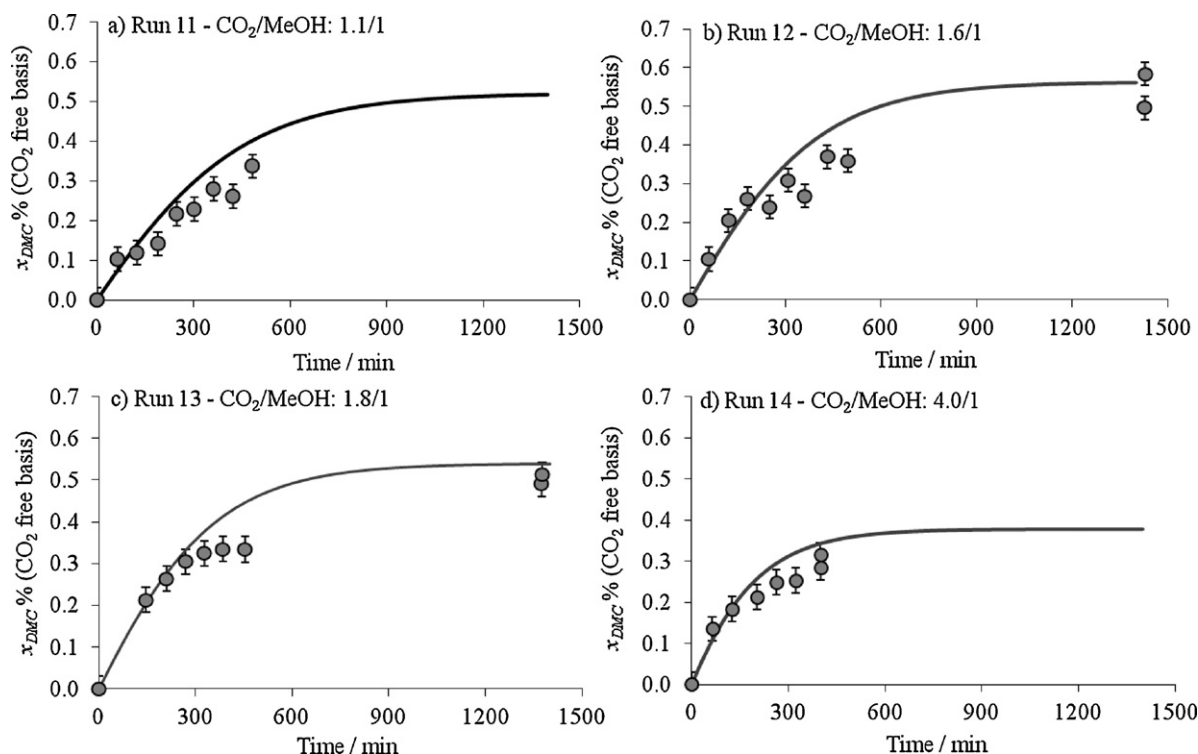**Fig. 8.** Experimental DMC molar fraction along the time at different $nCO_2/nMeOH$. Reaction conditions (approx.): 20.0 MPa, 398 K, 200 rpm, 4.6 g CeO_2.

carried out for a large range of $CO_2/MeOH$ ratio and temperature, which increases the fitting difficulty. Furthermore, the very low concentration of water and DMC leads to high relative deviation on the quantification method which may also contribute to these deviations.

The reaction rate is also affected by the pressure since it affects the equilibrium yield or by changing the partial pressure of each compound (Eqs. (4) and (5)). However, the pressure also affects the kinetic constant. The activation volume ($\Delta v^{\#}$) is the physical parameter that describes this effect, similar to the activation energy on the temperature effect. Eq. (9) expresses the effect of pressure on the kinetic constant [61].

$$k_p = \frac{k_{p0} \cdot \exp[-\Delta v^{\#} \cdot (P - P_0)]}{RT} \tag{9}$$

The activation volume of -0.24 ± 0.16 cm^3 mol^{-1} was adjusted from our experimental data (Runs 1, 16, and 17) using the same

objective function (Eq. (8)). The experimental and the predicted DMC molar fractions along the time for three different pressures are shown in Fig. 9. A drastic decrease on the DMC molar fraction at equilibrium conditions as well as on the reaction rate was observed by decreasing the pressure. A decrease around 30 and 40% on the DMC yield was observed for 17.5 and 15.0 MPa, respectively. The model prediction was significantly improved when considering the effect of pressure on the kinetic constant (activation volume).

4. Conclusions

In this work the kinetics for the direct synthesis of DMC over CeO_2 was investigated under high pressure conditions. The reaction experiments performed showed high reproducibility and were conducted under conditions that guarantee negligible external mass transfer resistances. The kinetic and equilibrium experiments were better modelled as ideal gas than considering real gas behaviour, using the SRK/mHV2 thermodynamic model from our previous work [18], probably due to the difficulty to predict the fugacity above the critical point. Furthermore, a standard enthalpy and Gibbs energy change of reaction equal to -20 ± 2 and 31 ± 1 kJ mol^{-1}, respectively, were adjusted from equilibrium data. The reaction rate model based on Langmuir–Hinshelwood mechanism showed lower deviations than the model based on Eley–Rideal mechanism. An activation energy of 106 ± 1 kJ mol^{-1} was fitted to the kinetic experiments, for the direct synthesis of DMC over CeO_2. Finally the effect of pressure on the reaction rate revealed an activation volume equal to -0.24 ± 0.16 cm^3 mol^{-1} (also adjusted to experimental data).

The developed kinetic model will be an important tool for the development and evaluation of novel processes, as reactive-separation technologies, which should be the most feasible engineering solution for the DMC sustainable production.
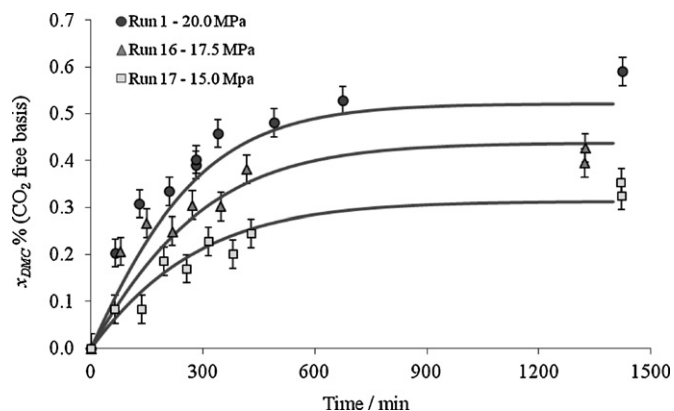

Fig. 9. Experimental DMC molar fraction along the time at different pressures. Reaction conditions (approx.): 398 K, 200 rpm, 4.6 g CeO_2, $nCO_2/nMeOH$: 2.5/1.

Acknowledgements

References

[1] D. Delledonne, F. Rivetti, U. Romano, Appl. Catal. A: Gen. 221 (2001) 241–251.
[2] S. Memoli, M. Selva, P. Tundo, Chemosphere 43 (2001) 115–121.
[3] A.A.G. Shaikh, S. Sivaram, Chem. Rev. 96 (1996) 951–976.
[4] Y. Ono, Appl. Catal. A: Gen. 155 (1997) 133–166.
[5] J.R. Ochoa-Gómez, O. Gómez-Jiménez-Aberasturi, B. Maestro-Madurga, A. Pesquera-Rodríguez, C. Ramírez-López, L. Lorenzo-Ibarreta, J. Torrecilla-Soria, M.C. Villarán-Velasco, Appl. Catal. A: Gen. 366 (2009) 315–324.
[6] B. Schäffner, F. Schäffner, S.P. Verevkin, A. Börner, Chem. Rev. 110 (2010) 4554–4581.
[7] M.A. Pacheco, C.L. Marshall, Energy Fuels 11 (1997) 2–29.
[8] U. Romano, R. Tesei, G. Cipriani, L. Micucci, US Patent 4218391 (1980).
[9] K. Nishihira, S. Yoshida, S.Tanaka, Y. Asada, US Patent 5631396 (1997).
[10] M. Sankar, C.M. Nair, K.V.G.K. Murty, P. Manikandan, Appl. Catal. A: Gen. 312 (2006) 108–114.
[11] B.M. Bhanage, S.I. Fujita, Y. Ikushima, M. Arai, Appl. Catal. A: Gen. 219 (2001) 259–266.
[12] G. Stoica, S. Abelló, J. Pérez-Ramírez, Appl. Catal. A: Gen. 365 (2009) 252–260.
[13] B. Yang, D. Wang, H. Lin, J. Sun, X. Wang, Catal. Commun. 7 (2006) 472–477.
[14] E. Leino, p. Mäki-Arvela, V. Eta, D.Y. Murzin, T. Salmi, J.P. Mikkola, Appl. Catal. A: Gen. 383 (2010) 1–13.
[15] T. Sakakura, J.C. Choi, Y. Saito, T. Sako, Polyhedron 19 (2000) 573–576.
[16] T. Sakakura, K. Kohno, Chem. Commun. (2009) 1312–1330.
[17] J.G.M.S. Monteiro, O. De Queiroz Fernandes Araújo, J.L. De Medeiros, Clean Technol. Environ. Policy 11 (2009) 209–214.
[18] B.A.V. Santos, V.M.T.M. Silva, J.M. Loureiro, D. Barbosa, A.E. Rodrigues, Fluid Phase Equilib. 336 (2012) 41–51.
[19] T. Sakakura, J.C. Choi, Y. Saito, T. Masuda, T. Sako, T. Oriyama, J. Org. Chem. 64 (1999) 4506–4508.
[20] J.C. Choi, K. Kohno, Y. Ohshima, H. Yasuda, T. Sakakura, Catal. Commun. 9 (2008) 1630–1633.
[21] S.T. Hong, H.S. Park, J.S. Lim, Y.W. Lee, M. Anpo, J.D. Kim, Res. Chem. Intermed. 32 (2006) 737–747.
[22] K. Kohno, J.C. Choi, Y. Ohshima, H. Yasuda, T. Sakakura, ChemSusChem 1 (2008) 186–188.
[23] K. Tomishige, K. Kunimori, Appl. Catal. A: Gen. 237 (2002) 103–109.
[24] B. Fan, H. Li, W. Fan, J. Zhang, R. Li, Appl. Catal. A: Gen. 372 (2009) 94–102.
[25] T. Sakakura, Y. Saito, M. Okano, J.C. Choi, T. Sako, J. Org. Chem. 63 (1998) 7095–7096.
[26] M. Honda, S. Kuno, N. Begum, K.I. Fujimoto, K. Suzuki, Y. Nakagawa, K. Tomishige, Appl. Catal. A: Gen. 384 (2010) 165–170.
[27] M. Honda, A. Suzuki, B. Noorjahan, K.I. Fujimoto, K. Suzuki, K. Tomishige, Chem. Commun. (2009) 4596–4598.
[28] M. Honda, S. Kuno, S. Sonehara, K.-i. Fujimoto, K. Suzuki, Y. Nakagawa, K. Tomishige, ChemCatChem 3 (2011) 365–370.
[29] V. Eta, P. Mäki-Arvela, A.-R. Leino, K. Kordás, T. Salmi, D.Y. Murzin, J.-P. Mikkola, Ind. Eng. Chem. Res. 49 (2010) 9609–9617.
[30] V. Eta, P. Mäki-Arvela, E. Salminen, T. Salmi, D.Y. Murzin, J.P. Mikkola, Catal. Lett. 141 (2011) 1254–1261.
[31] J.C. Choi, L.N. He, H. Yasuda, T. Sakakura, Green Chem. 4 (2002) 230–234.
[32] G. Laugel, X. Nitsch, F. Ocampo, B. Louis, Appl. Catal. A: Gen. 402 (2011) 139–145.
[33] K.T. Jung, A.T. Bell, Top. Catal. 20 (2002) 97–105.
[34] K. Tomishige, Y. Ikeda, T. Sakaihori, K. Fujimoto, J. Catal. 192 (2000) 355–362.
[35] M. Aresta, A. Dibenedetto, Dalton Trans. (2007) 2975–2992.
[36] D. Ballivet-Tkatchenko, S. Chambrey, R. Keiski, R. Ligabue, L. Plasseraud, P. Richard, H. Turunen, Catal. Today 115 (2006) 80–87.
[37] K. Tomishige, T. Sakaihori, Y. Ikeda, K. Fujimoto, Catal. Lett. 58 (1999) 225–229.
[38] K. Tomishige, H. Yasuda, Y. Yoshida, M. Nurunnabi, B. Li, K. Kunimori, Green Chem. 6 (2004) 206–214.
[39] K.W. La, J.C. Jung, H. Kim, S.H. Baeck, I.K. Song, J. Mol. Catal. A: Chem. 269 (2007) 41–45.
[40] Y. Ikeda, M. Asadullah, K. Fujimoto, K. Tomishige, J. Phys. Chem. B 105 (2001) 10653–10658.
[41] Y. Ikeda, T. Sakaihori, K. Tomishige, K. Fujimoto, Catal. Lett. 66 (2000) 59–62.
[42] H.J. Lee, S. Park, J.C. Jung, I.K. Song, Korean J. Chem. Eng. 28 (2011) 1518–1522.
[43] H.J. Lee, S. Park, I.K. Song, J.C. Jung, Catal. Lett. (2011) 1–7.
[44] M. Aresta, A. Dibenedetto, C. Pastore, C. Cuocci, B. Aresta, S. Cometa, E. De Giglio, Catal. Today 137 (2008) 125–131.
[45] T. Zhao, Y. Han, Y. Sun, Fuel Process. Technol. 62 (2000) 187–194.
[46] X.L. Wu, M. Xiao, Y.Z. Meng, Y.X. Lu, J. Mol. Catal. A: Chem. 238 (2005) 158–162.
[47] X.L. Wu, Y.Z. Meng, M. Xiao, Y.X. Lu, J. Mol. Catal. A: Chem. 249 (2006) 93–97.
[48] Y. Yoshida, Y. Arai, S. Kado, K. Kunimori, K. Tomishige, Catal. Today 115 (2006) 95–101.
[49] X.J. Wang, M. Xiao, S.J. Wang, Y.X. Lu, Y.Z. Meng, J. Mol. Catal. A: Chem. 278 (2007) 92–96.
[50] D. Ballivet-Tkatchenko, J.H.Z. dos Santos, K. Philippot, S. Vasireddy, C. R. Chim. 14 (2011) 780–785.
[51] J. Bian, X.W. Wei, Y.R. Jin, L. Wang, D.C. Luan, Z.P. Guan, Chem. Eng. J. 165 (2010) 686–692.
[52] A. Aouissi, A.W. Apblett, Z.A. Al-Othman, A. Al-Amro, Transition Met. Chem. (2010) 1–5.
[53] A. Aouissi, Z.A. Al-Othman, A. Al-Amro, Int. J. Mol. Sci. 11 (2010) 1343–1351.
[54] J. Bian, X.W. Wei, L. Wang, Z.P. Guan, Chin. Chem. Lett. 22 (2011) 57–60.
[55] V. Eta, P. Mäki-Arvela, J. Wärnå, T. Salmi, J.P. Mikkola, D.Y. Murzin, Appl. Catal. A: Gen. 404 (2011) 39–46.
[56] H.J. Hofmann, A. Brandner, P. Claus, Chem. Ing. Tech. 83 (2011) 1711–1719.
[57] J.M. Smith, H.C.V. Ness, M.M. Abbott, Introduction to Chemical Engineering Thermodynamics, sixth ed., McGraw-Hill, NY, 2005.
[58] K.T. Jung, A.T. Bell, J. Catal. 204 (2001) 339–347.
[59] J.L. Figueiredo, F.R. Ribeiro, J.J.M. Orfão, F. Lemos, M. Guisnet, Catálise Heterogénea, 2ª ed. rev. e actualizada ed., Fundação Calouste Gulbenkian. Serviço de Educação e Bolsas, Lisboa, 2007.
[60] B. Efron, Ann. Stat. 7 (1979) 1–26.
[61] A.B.G. Vetter, High Pressure Process Technology: Fundamentals and Applications, first ed., Elsevier Science B.V., Amsterdam, 2001.